RSC Advances

ROYAL SOCIETY OF CHEMISTRY

www.rsc.org/advances

Carbon dioxide stripping through water by porous PVDF/Montmorillonite hollow fiber mixed matrix membranes in a membrane contactor

M. Rezaei DashtArzhandi[a], A. F. Ismail[a,*], T. Matsuura[a,b]

[a]Advanced Membrane Technology Research Centre (AMTEC), Universiti Teknologi Malaysia, 81310 Skudai, Johor, Malaysia

[a,b]Industrial Membrane Research Institute, Department of Chemical and Biological Engineering, University of Ottawa, 161 Louis Pasteur St., Ottawa, ON, K1N 6N5, Canada

[*]Corresponding author email: afauzi@utm.my

Tel.: +60 7 5535592; fax: +60 7 5581463

Abstract

Hydrophobic Montmorillonite (MMT)-filled polyvinylideneflouride (PVDF) hollow fiber mixed matrix membranes (MMMs) were fabricated by means of wet phase inversion method to meet the requirements of stripping process at elevated temperatures via membrane contactor. The effects of MMT incorporation into polymer matrix in different loadings (1, 3, 5 wt% of polymer) on the membrane properties and CO_2 stripping flux and efficiency were investigated. The incorporation affected the phase inversion process and accelerated the exchange rate of solvent/coagulant, resulting in formation of membranes with longer finger-like pores and higher surface porosity. In addition, the MMMs exhibited higher contact angle and wetting resistance than plain membrane. As a result, physical CO_2 stripping flux from water and process efficiency became significantly higher than the plain PVDF hollow fiber with maximum achieved when 5 wt% MMT (coded as M5) was embedded in the polymer. The highest stripping flux of 4.19×10^{-3} mol m^{-2} s^{-1} was achieved by M5 at the tested temperature of 27 °C and the liquid velocity of 2.8

m s^{-1}, which was 38% higher than the plain PVDF hollow fiber at the same operating conditions. A significant stripping performance enhancement was also observed by increasing the temperature of CO_2 rich liquid from 27 to 45 and 80 °C.

These results suggest that the impregnation of polymeric membranes by inorganic hydrophobic clay particles can be an effective method to improve the morphology and performance of PVDF hollow fibers in CO_2 stripping via gas-liquid membrane contactor.

Keywords: Carbon dioxide stripping, Mixed matrix membrane contactor, Wettability, Absorbent temperature, Montmorillonite nano-clay

1. Introduction

The removal of acid gases, particularly carbon dioxide (CO_2), from flue gas and natural gas has become a worldwide concern over the last few years due to growing evidence of their effect on global climate changes [1]. Conventionally, CO_2 capture is implemented by a number of processes. Among those, one of the most widely used technique is absorption/desorption using liquid absorbents in traditional equipment including packed columns, bubble columns, and spray towers [2]. Typically, the process is conducted in two separated towers, absorption and stripping processes. In the first absorption tower, the liquid absorbent flows from the top, removing CO_2 from the gas that flows counter-currently from the bottom of the tower to come into contact with the liquid. Then the CO_2 rich solvent is regenerated at the second tower at slightly above normal pressure and high temperature. These processes have many deficiencies owing to their direct contact of gas and liquid such as flooding, loading, entrainment and channeling that contribute to reduction of mass transfer [3]. Moreover, they need considerable energy consumption and

operating costs are high [4, 5]. Indeed, the priority should be given to the development of highly effective technologies that are able to minimize overall environmental and economical impacts. Membrane contactor for CO_2 capture using porous hollow fibers has been researched extensively over the past few decades as an alternative process to suppress disadvantages of the conventional equipment [2]. Membrane contactors have high surface area per unit volume ratio, enabling reduction of capital cost and energy consumption. They do not have the problems of flooding, loading and channeling due to non-dispersive gas and liquid flows. They also enjoy high flexibility and modularity which provide performance superior to conventional methods [6-8]. The absorption of unwanted gas (CO_2 or H_2S) through a membrane contactor occurs when the gas contacts with the liquid phase flowing on the opposite side of a hollow fiber membrane that acts as a barrier. Hence, gas and liquid in contrast to conventional absorption and desorption devices are manipulated independently. CO_2 rich liquid then comes into contact with a stripping gas in the next contactor to remove CO_2 from the liquid and regenerate the liquid absorbent as shown schematically in Fig. 1 [9, 10]. Even though the CO_2 stripping is a vital section of the absorption/desorption processes, only scarce information, in contrast to the vast works done on the absorption, is available in the literature on the desorption side [11, 12]. This might be due to the limitation of polymeric membrane materials that can not withstand an elevated temperature required for stripping [13]. As known, high pressure and low temperature can favor absorption process, while low pressure and high temperature are effective parameters in regeneration of rich CO_2 solutions. However, polymeric membrane contactors are usually designed to be applied in mild operating conditions such as low temperature and pressure [14]. Therefore, an effort should be made to explore new membrane materials or to stabilize existing polymeric materials at harsh conditions. As for polymeric membrane materials, they are limited to fluoropolymers such as

polythetrafluoroethylene (PTFE). For example, Kumazawa [15] and Khaisri, et al. [16] fabricated PTFE hollow fiber membranes for chemical CO_2 stripping via membrane contactor. However, PTFE is expensive and its processability is poor due to weak solubility in common solvents at ambient temperature. Alternative to PTFE, Simioni, et al. [3] utilized plasma sputtered nylon membrane to strip CO_2 at elevated temperatures with aqueous potassium carbonate as absorbent. The plasma sputtered membrane showed superior CO_2 stripping performance at all tested temperatures, however, the membrane experienced a significant performance deterioration at high temperatures of 90-100 °C due to intrusion of solvent in membrane pores and pore wetting influences. The membrane mass transfer resistance was reported to be 72% of total mass transfer resistance at high operating temperatures. Polyvinylideneflouride (PVDF) as the only hydrophobic polymer, soluble in solvents at normal temperatures can be easily converted to asymmetric membranes via phase inversion method allowing excellent control on pore size ad porosity. However, this polymer also has some shortcomings. The viscosity of PVDF, when dissolved in a solvent, is high, which can limit the penetration of the coagulant into the nascent membrane during the phase inversion process [17]. In addition, the surface hydrophobicity of this polymer is not as high as other fluoropolymers, which requires improvement. Another problem is relatively high susceptibility to degradation at high temperature, which is related to the presence of fluorine in the structure [18]. Hence, it seems crucial to modify PVDF to fulfill the requirements of stripping process at an elevated temperature. Naim, et al. [19] improved the structure of PVDF hollow fiber membrane by addition of lithium chloride (LiCl) in spinning dopes for chemical CO_2 stripping from aqueous diethanolamine (DEA) solution via contactor system. The asymmetric membranes fabricated via phase inversion method showed a linear increase of stripping flux and efficiency with LiCl concentration in the polymer dope. However, the

hydrophobicity of membrane surface decreased by increasing LiCl content. Rahbari-Sisakht, et al. [20] modified PVDF hollow fiber membrane by incorporation of surface modifying macromolecules (SMMs) into spinning solution. The hydrophobicity of membrane was increased but its enhancement occurred along with increasing membrane pore size and decreasing wetting resistance, which rendered the long-term stability of the process undesirable.

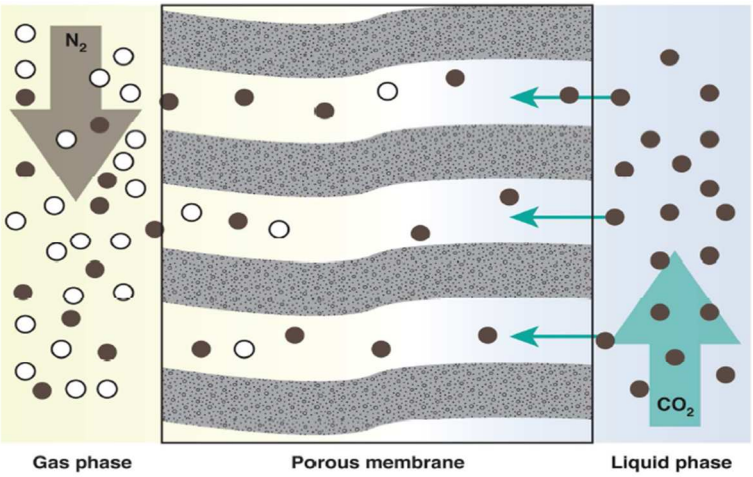

Fig. 1: Mechanism of CO_2 stripping through gas-liquid membrane contactor

Mixed matrix membranes (MMMs), consisting of inorganic fillers dispersed in a polymer matrix, are known to combine the advantages of both organic and inorganic phases. Inorganic nano-fillers having high thermal and chemical stability, porosity and surface area give excellent properties to the nanocomposite membranes [21-23]. They can function as morphological modifiers and also improve the surface hydrophobicity/philicity [24]. Most studies published so far indicated the favorable effect of incorporated inorganic particles on both membrane surface properties (e.g. pore size, surface porosity and roughness) and the morphology of the membrane sublayer [25-29]. Therefore, demand on MMMs as a unique ceramic-polymeric membrane has been increased.

Utilization of organic/inorganic membranes in the absorption/desorption application may also prove to be an effective way to overcome the aforementioned drawbacks of the polymeric membrane materials. In the design of MMMs, the organic/inorganic materials should be selected based on the requirements specific to the process [30, 31]. It has been reported that many properties of PVDF membranes such as thermal, chemical and mechanical stabilities and also membrane gas permeance and wetting resistance were improved by incorporation of montmorillonite (MMT) nano-clay filler [32]. MMT nano-clay is a lamellar layered material with a high aspect ratio [33]. Wang, et al. [34] improved the hydrophilicity of PVDF membrane by hydrophilic MMT. They revealed that the addition of a small amount of MMT and polyvinypyrrolidone (PVP) has strong effects on the membrane pore shape, pore size, porosity and permeability. In another work, they improved the properties of PVDF hollow fiber membranes for direct contact membrane distillation (DCMD) by the addition of MMT into PVDF spinning solutions [24]. The fabricated composite membranes could withstand longer operation time without detecting any membrane degradation or deformation and keep more stable vapor permeation flux than plain PVDF membrane due to the obtained unique membrane morphology.

In our previous works, highly porous and hydrophobic PVDF/MMT hollow fiber MMMs were fabricated via wet phase inversion method. The membranes exhibited high performance and promising long-term test results for CO_2 absorption via membrane contactor [9, 35, 36]. The objective of this work is to use the prepared PVDF/MMT hollow fiber MMMs for the CO_2 stripping process via membrane contactor. To the best of our knowledge no research has been done on the utilization of hollow fiber MMMs in CO_2 stripping. The effects of MMT loading and some operating parameters such as liquid velocity and absorbent temperature on the CO_2 stripping performance and process efficiency are investigated.

2. Experimental

2.1. Materials

Commercial PVDF polymer pellets (Kynar® 740, Arkema Inc., PA, USA) were used as the base polymer. 1-Methyl-2-pyrrolidone (N-Methyl-2-pyrrolidone, NMP, 99.5%) was used as the solvent without further purification. Hydrophobic MMT and nanomer 1.30TC were purchased from Fluka and used as received.The clay was organically modified by octadecylamine (25–30 wt%) and then was treated with ammonium ions. The structure of quaternary ammonium ions is $N^{+}(CH_2CH_2OH)_2(CH_3)HT$, where HT, the hydrogenated tallow, is composed of 65% $C_{18}H_{37}$, 30% $C_{16}H_{33}$, and 5% $C_{14}H_{29}$. In general, the clay particle surface dimensions ranged from 300 to more than 600 nm, length/thickness ratio = 200–300, specific surface area = 750 m^2/g. LiCl with purity more than 99% was purchased from Sigma–Aldrich® and used as non-solvent additive in the polymer solution. Distilled water was used as the representative absorbent in physical stripping test. Pure CO_2 and N_2 gas were employed as the solute gas and the sweep gas, respectively.

2.2. Fabrication of asymmetric hollow fiber membranes

Four polymer solutions consisting of PVDF/NMP/LiCl (18/2.5/79.5 wt%) and different contents of modified MMT nano-clay (0, 1, 3, 5 wt% of polymer) were prepared. The PVDF polymer was gradually added to the prepared suspension of MMT in the NMP/LiCl mixture under vigorous stirring for at least18 h at 50 °C to ensure the complete dissolution of the polymer. The solutions were ultra-sonicated, degassed and maintained at room temperature for at least 2 h before spinning to remove air bubbles in the solution. The hollow fiber spinning by the phase inversion process was described elsewhere in detail [37]. The flow rate of the spinning dope through the

spinneret was maintained at 4.5 ml min^{-1} using nitrogen pressure while the bore fluid (20/80 wt ratio of water/NMP) flow rate was maintained at 1.7 ml min^{-1}. Tap water was used as the external coagulant to solidify the nascent hollow fibers. The spun fibers were immersed in water for 3 days with daily change of water to remove the residual solvent and the non-solvent additive. Then, the hollow fibers were post-treated by immersion in methanol for 15 min before drying. The MMMs were subsequently dried at ambient temperature for further experiments. Depending on the MMT content in MMM the hollow fibers are named as M0, M1, M3 and M5, where the digit following M is the MMT wt% in polymer.

2.3. Membrane characterization

2.3.1. Field emission scanning electron microscopy (FESEM)

The fabricated hollow fiber membranes were cut into the length of 5 cm, immersed in liquid nitrogen and fractured, then positioned on a holder and sputtered with platinum before testing. Field emission scanning electron microscopy (FESEM) (JEOL JSM-6701F) images from outer/inner hollow fiber membrane surfaces and their cross section were taken under various magnifications.

2.3.2. Gas permeation test and collapsing pressure measurement

The pore size and the effective surface porosity (surface porosity over effective pore length) for a porous asymmetric membrane is important characterization parameters. These parameters were hence obtained using the conventional nitrogen gas permeation test. The details of the permeation test are described elsewhere [38]. Three hollow fibers with an effective length of 10 cm were placed in a stainless steel housing with one end sealed and the other end open for N_2 gas

inlet. Pure nitrogen (N_2) was used as the test gas and the gas flow rate was measured by a bubble flow meter. Then, the gas permeance was calculated based on the inner diameter of hollow fibers at ambient temperature.

The method of calculating mean pore size and effective surface porosity from the experimental permeance data by assuming cylindrical pores in the skin layer of the asymmetric membrane is as follows. The gas permeance is given a combination of both the Poiseuille and Knudsen flow as [39]:

$$\bar{P} = P_p + P_k = \left(\frac{2}{3}\right)\left(\frac{8RT}{\pi M}\right)^{0.5} \frac{r_{p,m}}{RT}\frac{\zeta}{L_p} + \frac{1}{8\mu}\frac{r_{p,m}^2}{RT}\frac{\zeta}{L_p}\bar{p} \quad \textbf{(1)}$$

$$\bar{P} = A + B\bar{p} \quad \textbf{(2)}$$

where $\bar{P}$ is the total gas permeance (mol m^{-2} Pa^{-1} s^{-1}), P_p and P_k are the gas permeance by Poiseuille and Knudsen flow, respectively, R is the universal gas constant (8.314 J mol^{-1} K^{-1}), T is the absolute temperature (K), M is molecular weight of gas (kg mol^{-1}), $r_{p,m}$ is the mean pore radius (m), μ is the viscosity of gas (Pa s), ζ is surface porosity, L_p is the effective pore length (m) and $\bar{p}$ is mean pressure (Pa) ($(p_u + p_d)/2$ where p_u is upstream pressure and p_d is downstream pressure). The upstream pressure was in the range from 3.5×10^5 to 8×10^5 Pa (from 3.5 to 8 bar) (gauge). Using the intercept (A) and the slope (B) of the straight line of $\bar{P}$ versus $\bar{p}$ plot according to Eqs. 1-2, the mean pore size and the effective surface porosity can be calculated by the following equations [31, 40, 41].

$$r_p = \frac{16}{3}\frac{B}{A}\left(\frac{8RT}{\pi M}\right)^{0.5}\mu \quad (3)$$

$$\frac{\zeta}{L_p} = \frac{8\mu RTB}{r_{p,m}^2} \quad (4)$$

It should be mentioned that the calculated pore size and the effective surface porosity do not have any significant physical meaning but they can be used as a criterion for comparing the membranes fabricated under different spinning conditions [6].

2.3.3. Liquid Entry Pressure of Water (LEPw) and Contact Angle Measurement

Liquid entry pressure of water (LEPw) and contact angle measurement were conducted to evaluate wetting resistance of fabricated membranes. LEPw is the minimum pressure required to drive the liquid through the membrane pores and the membranes used in membrane contactor should have sufficient LEPw to prevent intrusion of absorbents into membrane pores. For measuring LEPw, the same modules as those used for the gas permeation test were prepared. Distilled water was fed into the lumen side of hollow fibers and the pressure slowly increased with a step size of 0.5 bar. At each pressure, the membrane module was left for at least 15 min to check if any water permeates into the fiber shell side. The LEPw was reported as the pressure when the first water droplet appeared on the outer surface of hollow fibers.

The sessile drop technique with a goniometer (model G1, Krüss GmbH, Hamburg, Germany) was used to measure the contact angle of the hollow fibers' outer surface. The contact angle measurement at minimum ten various positions was required to obtain a reliable average value since the hollow fiber diameter was small.

2.4. CO_2 Stripping Test

The physical CO_2 stripping test for the plain PVDF and MMM hollow fibers was conducted in a contactor system. The contactor module containing ten hollow fibers with an effective length of 17.5 cm were prepared. Table 1 shows the specifications of the prepared contactor module used in the stripping test. Distilled water was saturated with CO_2 before entering into the lumen side of the hollow fiber membrane modules for the stripping test.

Table 1: Characteristics of membrane contactor module.

Module i.d. (mm)	14
Module length (mm)	250
Fiber o.d. (μm)	800-850
Fiber i.d. (μm)	430-480
Effective fiber length (mm)	175
Number of fibers	10

Heating of the rich CO_2 solution to 27 °C, 45 °C and 80 °C was performed by a heater with digital controller (Protech, model 83) before entry into the stripping modules. Pure nitrogen was used as sweep gas and flowed in the shell side of the module in a counter current mode at a constant flow rate of 1.2 ml min^{-1}. Liquid side pressure was maintained 0.5 bar higher than the gas side by using control valves installed at the module inlet and outlet of both liquid and gas streams to prevent bubbling of gas into the liquid. The CO_2 concentration of the liquid stream at different temperatures in the inlet and outlet of the stripping module was measured by chemical titration method using 0.02 molar sodium hydroxide (NaOH) solution as titrant and phenolphthalein as indicator to evaluate the stripping flux and system efficiency. Fig. 2 shows the flow diagram of the stripping test setup.

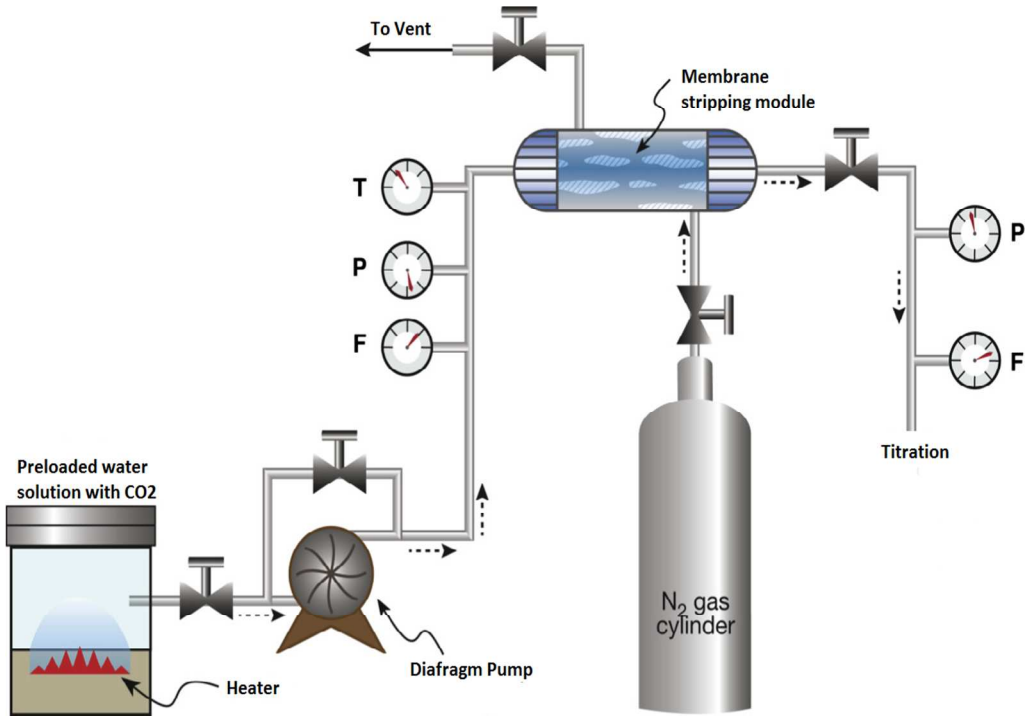

Fig. 2: Flow diagram of experimental CO_2 stripping membrane contactor system.

The CO_2 stripping flux was calculated based on the inner surface area of the hollow fibers by:

$$J_{CO_2} = \frac{(C_{l,in} - C_{l,o}) \times Q_l}{A_i} \quad \textbf{(5)}$$

where J_{CO_2} is the CO_2 stripping flux (mol m^{-2} s^{-1}), $C_{l,in}$ and $C_{l,o}$ are the liquid phase CO_2 concentrations in the inlet and outlet of the membrane modules (mol m^{-3}), respectively, Q_l is liquid flow rate (m^3 s^{-1}) and A_i is the inner surface of the hollow fiber membranes (m^2). The CO_2 stripping efficiency (η) of hollow fiber membranes was obtained by following equation:

$$\eta(\%) = \left(1 - \frac{C_{l,o}}{C_{l,in}}\right) \times 100 \quad (6)$$

3. Results and discussion

3.1. Morphological studies

Porous hollow fiber membranes with different hydrophobic MMT nano-clay contents were fabricated via wet phase inversion method for CO_2 stripping through membrane contactor. It is well known that the most important parameters of the phase inversion process are thermodynamic stability of polymer solution and kinetics of mutual solvent-coagulant exchange. They are responsible for triggering the changes in membrane morphology, permeability and CO_2 stripping performance. These parameters were critically affected by incorporation of MMT nano-clay into PVDF polymer solutions. The addition of MMT caused polymer solution to experience lower viscosity (see Table 2) which consequently decreased thermodynamic stability and accelerated demixing rate of solvent/coagulant during spinning [42]. The lower viscosity was due to presence of surface modifier (tallow) used for surface modification of clay particles in the system. The solution with the highest MMT content (5 wt%) possessed the lowest viscosity (Table 2). Therefore, the addition of clay particles to the PVDF solutions affected the mechanism of membrane formation in the water bath and induced changes in both the membrane skin layer and the membrane sublayer morphology.

Figure 2 depicts the FESEM images of the cross-section, outer and inner surfaces of the plain PVDF membrane and hollow fiber MMM with 5 wt% MMT (M5) representing all mixed matrix membranes' morphology. From the cross-sectional images (Figs. 2(A1), 2(B1)), it can be seen that MMMs have longer finger-like pores which meet with a thick sponge-like layer in the middle of the membranes. The formation of longer finger-like macrovoids for MMMs was due to

less thermodynamic stability and faster liquid-liquid demixing caused by addition of clay particles [43]. In addition, a thick sponge-like layer in the middle of the cross-section is caused by less penetration of water into this region. The longer finger-like pores of MMMs make the sponge-like layer thinner leading to higher permeation rates of MMMs. Furthermore, the tear-like macrovoids observed in plain PVDF hollow fiber membrane have almost disappeared in MMMs. It confirms that the pores had less time to merge and grow in size as demixing rate was increased by addition of clay particles.

The FESEM images of the inner surface (Figs. 2(A2), 2(B2)) show large pores, although they might not necessarily be penetrating through the hollow fibers' cross-section. The solvent power of bore fluid that is stronger than water did not allow the formation of skin layer at the inner surface [30, 44, 45].

Regarding the outer surface micrographs (Figs. 2(A3), 2(B3)), the surface looks much smoother than the inner surface, indicating the formation of skin layer due to the fast diffusion rate of solvent and fast phase inversion rate. The outer surface of the MMMs is slightly rougher than the outer surface of plain PVDF hollow fiber, but there is no indication of particle agglomeration [24, 34, 46]

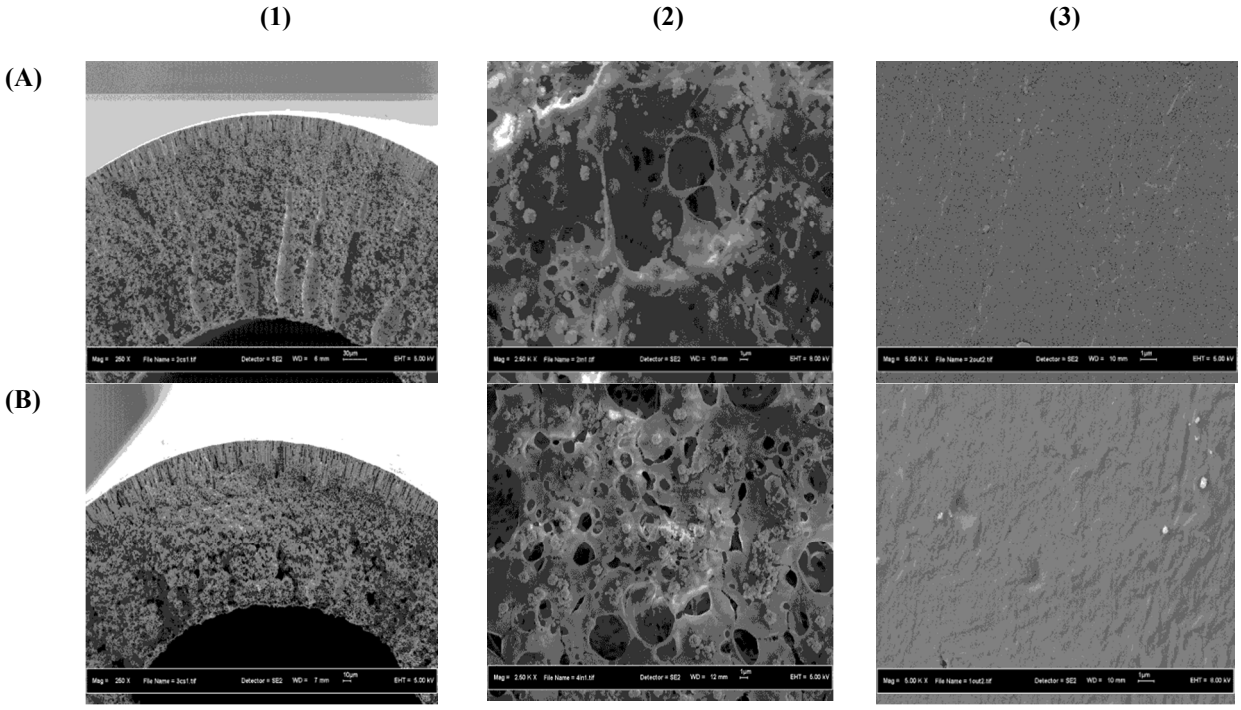

Fig. 2: FESEM morphology of the PVDF hollow fiber membranes: (A) plain PVDF (M0); (B) MMM hollow fiber (M5); (1) cross section; (2) inner surface; and (3) outer surface.

N_2 permeance, mean pore size and effective surface porosity obtained from the gas permeation tests of the fabricated membranes are presented in Fig. 3 and Table 2. It is obvious that the gas permeance of membranes increased by addition of MMT to PVDF dopes showing a maximum at M3. The higher permeation rates of MMMs are in accordance with the formation of longer finger-like macrovoids. In Table 2, the effective surface porosity increases progressively with MMT clay loading. Pore size of membranes slightly increased by adding MMT, but interestingly, the pore size of M5 was even smaller than M0. This was the reason why the M5 exhibited slightly lower permeance than M3 despite its larger effective surface porosity.

Table 2: Characteristics of the fabricated hollow fiber membranes.

Membrane No.	M0	M1	M3	M5
Polymer solution viscosity (centipoise)	1250	740	665	590
Permeance of N_2 gas at 7 bar_g (10^{-7}mol/m^2s Pa)	3.68	6.63	8.74	7.70
Effective surface porosity (m^{-1})	87	124	171	237
Mean pore size, $r_{P,m}$ (*nm*)	26	32	34	22
LEPw (bar)	8 ± 0.5	9.5 ± 0.3	9 ± 0.5	11 ± 0.5
Contact angle (Θ)	80° ± 1.5	84° ± 1.25	88° ± 1.5	99° ± 1.5
Stripping flux (mol m^{-2} s^{-1}) 27 °C[a]	2.6×10^{-3}	--	--	4.19×10^{-3}
Stripping flux (mol m^{-2} s^{-1}) 45 °C[a]	5.6×10^{-3}	--	--	6.99×10^{-3}
Stripping flux (mol m^{-2} s^{-1}) 80 °C[a]	6.87×10^{-3}	--	--	7.55×10^{-3}

a: at the highest liquid velocity of 2.8 m s^{-1}

1

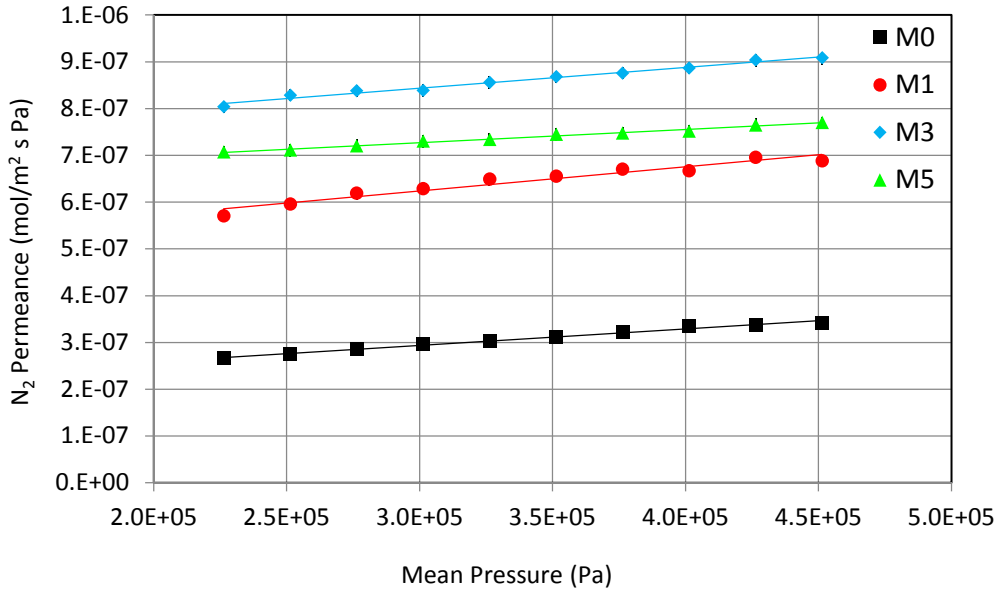

Fig. 3: Measured N_2 permeance of membranes as a function of mean pressure.

High membrane hydrophobicity and wetting resistance are crucial factors in membrane stripping. The high wetting resistance prevents the pore wetting and contributes to stable contactor performance in long-term operations. The contact angle measurement using sessile drop method is commonly considered as a simple and convenient method of obtaining qualitative information about membrane surface hydrophobicity [28]. The contact angle of hollow fiber membranes increases from 80° of M0 to 99° of M5 (see Table 2). It can be related to the increase of effective solid surface area and interfacial energy between the solid and liquid by the addition of hydrophobic nano-fillers in the system [47]. In other words, the presence of the clay particles in the system reduced surface energy of the membrane. It is well known that the solid surfaces having lower surface energy have greater contact angle [48].

Liquid entry pressure of water (LEPw) as an indicator of membrane pore wetting is influenced by membrane hydrophobicity and pore size [49]. The MMMs demonstrated higher wetting resistance than plain membrane with the highest 11 bar of M5 (see Table 2). It is ascribed to the observed highest surface hydrophobicity and the smallest pore size of M5 which restrict the absorbent intrusion into membrane pores.

Since surface porosity, hydrophobicity and wetting resistance of membranes were significantly improved by the addition of MMT, higher stripping performance and efficiency of MMMs can be expected.

3.2 CO_2 stripping test

In the CO_2 stripping test, emphasis is on the effects of liquid flow rate and rich CO_2 solution temperature on the CO_2 stripping flux and process efficiency. CO_2 rich liquid was supplied into the lumen side of the hollow fiber since the membrane stripping process is known to be a liquid phase rate controlled process and the flow velocity can be higher in the lumen side than in the

shell side [10]. Simioni, et al. [50] increased CO_2 stripping performance of PTFE and polyethersulfone (PES) flat sheet membranes by installing a stirrer in the liquid side to increase the turbulence. In addition, practically no change of stripping flux has been reported by increasing gas flow rate [11, 15, 16]. For example, Mansourizadeh [51] reported an almost constant physical CO_2 stripping flux when the gas velocity was increased from 0.01 to 0.05 m s^{-1}. It is noteworthy that the effect of gas flow rate was also insignificant in CO_2 stripping where an aqueous solution containing an organic compound was used as the absorbent [16].

Fig. 4 presents the CO_2 stripping flux as a function of liquid velocity for all the fabricated membranes at fixed operating temperature and pressure (27 °C and 1.3 bar respectively) with N_2 as stripping gas. As can be seen, the flux increases with increasing liquid velocity for all fabricated membranes due to decrease in liquid boundary layer resistance, which contributed to decrease of the overall mass transfer resistance [7]. A linear dependency of stripping flux and liquid velocity is also reportaed for chemical stripping of CO_2 from aquous MEA solution in PTFE hollow fibermembrane contactor [16].

The stripping flux also increased progressively from M0 to M5, as the filler loading increased. The increase of stripping flux from plain PVDF hollow fibers (M0) to the hollow fiber MMMs is in accordance with FESEM observations, N_2 permeance and wetting resistance results; i.e. MMMs having higher surface porosity, hydrophobicity and LEPw exhibited higher performance than plain membrane. Indeed, higher porosity of MMMs allows higher CO_2 gas permeation through the pores and higher wetting resistance suppress water intrusion into the MMMs' pores, allowing MMMs to maintain fast CO_2 gas permeation through the membrane pores. Moreover, as observed in the cross-sectional FESEM images, MMMs possess longer finger-like pores, which minimize the contribution of sponge-like layer to the CO_2 gas permeation resistance.

However, it is reported sometimes that the hollow fiber membranes with large finger-like macrovoids are not desired for gas-liquid contacting processes and might lead to increase membrane pore wetting [52].

It is interesting to note that M5 exhibited lower N_2 gas permeance than M3. While the CO_2 stripping flux of M5 is higher than M3. This is most-likely attributed to the smaller pore size of M5 in comparison to M3 (see Table 2), i.e. the larger pores of M3 were partially wetted in the stripping experiments which reduced the CO_2 flux, while pore wetting of M5 was prevented more effectively by its smaller pore size.

The highest stripping flux at the tested temperature of 27 °C and liquid velocity of 2.8 m s^{-1} of 4.19×10^{-3} mol m^{-2} s^{-1} was obtained for M5 MMM, which was approximately 38% higher than the plain PVDF at the same operating conditions (see Fig. 4 and Table 2). Mansourizadeh [51] fabricated PVDF hollow fiber membranes for CO_2 stripping from water via membrane contactor. Their reported stripping flux was significantly lower than the flux of M5 MMM in this study under the same operating conditions. The lower performance could be ascribed to the larger pore size of 280 nm and low LEPw (2.5 bar) of their fabricated membrane, which resulted in more pore wetting and mass transfer resistance. Rahbari-Sisakht, et al. [20] improved hollow fiber PVDF membrane by blending hydrophobic surface modifying macromolecules (SMMs) to enhance CO_2 stripping performance through water. The highest stripping flux of 2.1×10^{-3} was achieved for the surface modified PVDF membrane containing 6% SMM into dope which was almost 99 % lower than the stripping flux of M5 MMM. It was most likely related to the increased membrane mean pore size from 158 to 654 nm and consequent low LEPw by blending SMM. Therefore, as an additive, MMT inorganic clay particle is superior to SMM.

Interestingly, unlike several works in the literature which reported leveling off of the stripping flux even at low liquid velocities of 0.3 m s^{-1} process [51, 53, 54], the stripping flux of the MMMs fabricated in this work kept increasing even at the highest flow rate of 2.8 m s^{-1} (see Fig. 4). This indicates low resistance of MMMs and the dominant liquid boundary layer resistance on the overall resistance.

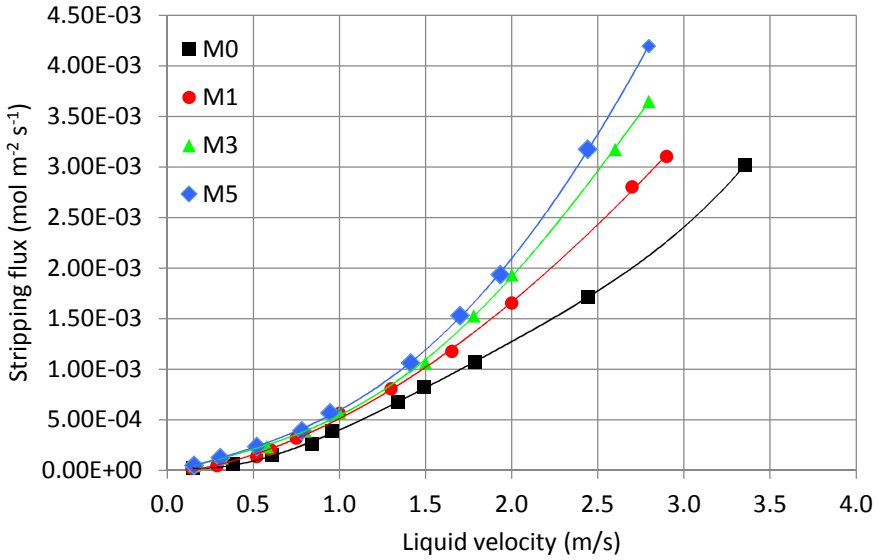

Fig. 4: Effect of liquid velocity on stripping flux (T = 27 °C).

The stripping efficiency was calculated by Eq. (6) and the results shown in Fig. 5. The stripping efficiency also increased by increasing liquid velocity and clay loading. The highest stripping efficiency of 23 % at the temperature of 27 °C was achieved by M5 at the liquid velocity of 2.8 m s^{-1} which was 64% higher than the plain PVDF hollow fiber (M0).

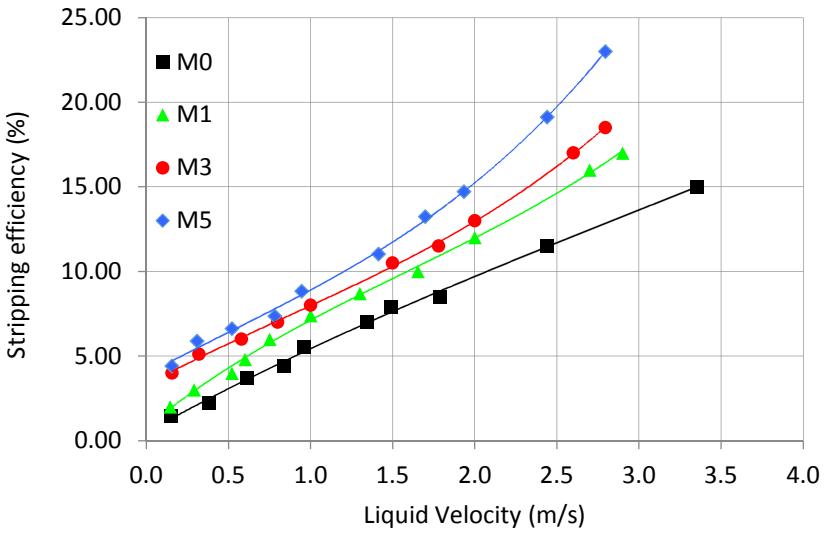

Fig. 5: Effect of liquid velocity on stripping efficiency (T = 27 °C).

As the M5 MMM exhibited the highest stripping flux and process efficiency among all fabricated membranes, the effect of rich CO_2 solution temperature on the stripping flux of M5 and M0 was measured and the results were compared as presented in Fig. 6. In Fig. 6 the CO_2 loaded liquid temperature has a direct influence on the CO_2 desorption performance. The stripping flux increases by increasing temperature at any adjusted liquid velocity. In fact, increasing temperature lowered the dissolved CO_2 concentration in water at equilibrium, resulting in an increase in driving force for mass transfer. The flux increase also is due to decreasing rich CO_2 solution viscosity and surface tension by increase in temperature, resulting in faster diffusion rate and further stripping performance enhancement [13, 50]. The viscosity of water decreases from 0.9×10^{-3} to 0.36×10^{-3} Pa.s [55] and surface tension decreases from 7.2×10^{-2} to 6.3×10^{-2} N/m [56] when the temperature increases from 27 to 80 ºC. Consequently, the stripping flux of M5 from 4.19×10^{-3} at ambient temperature (27 ºC) considerably increased to

the highest value of 7.55×10^{-3} mol m^{-2} s^{-1} at the liquid temperature of 80 °C and velocity of 2.8 m s^{-1} (see Table 2 and Fig. 6).

However, the flux also possible to decrease or become constant particularly at high operating temperatures. This is because of decreasing liquid surface tension and viscosity by temperature which increase the possibility of membrane pore wetting by solvent intrusion [50]. The interpretation could be supported by a comparison between the obtained stripping fluxes at low and high tested temperatures. The stripping flux enhancement of M5 when the absorbent temperature was increased form 27 °C to 45 °C was 67%, while only 8% was the enhancement where the absorbent temperature increased from 45 °C to 80 °C (see Fig. 6 and Table 2). It is obvious that the stripping flux improvement at low temperatures is significantly greater than high temperature operations. Therefore, it can be concluded that the enhancement effect of temperature on stripping flux above a specific absorbent temeperture is counterbalanced by membrane pore wetting. In addition, the membrane wetting and subsequent flux decrease at high operating temperatures could be related to the possible membrane morphological changes above that specific temperature, which as an objective will be invesigated in our future communications. The specific temperature value is suggested to be recognized based on the membrane structure and hydrophobicity. Naim, et al. [7] fabricated PVDF membranes for CO_2 stripping via membrane contactor and the results revealed that the stripping flux increases by increasing both liquid velocity and temperature. However, they detected significant performance deterioration at high temperature of 80 °C. The authors related the performance decline to the membrane pore wetting, which caused the membrane resistance to become dominant.

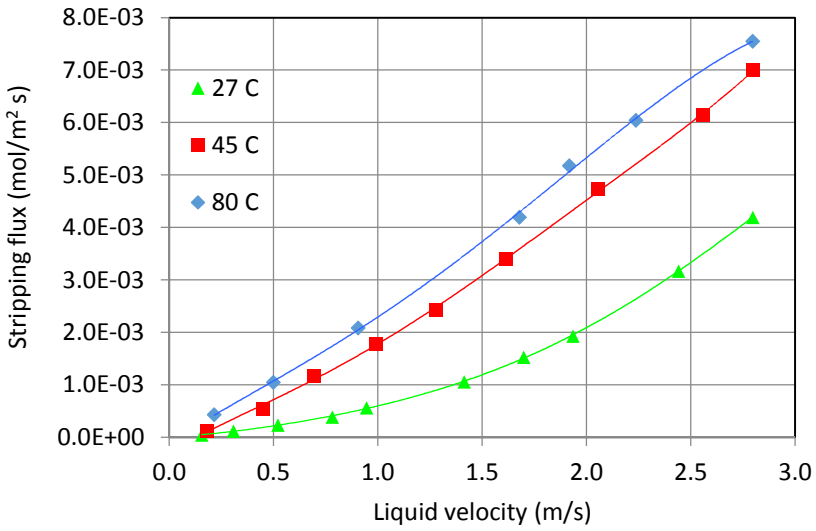

Fig. 6: Effect of rich solution temperature on CO_2 stripping flux of M5 MMM.

Furthermore, the M5 MMM exhibited better CO_2 stripping flux than plain membrane at elevated rich CO_2 solution temperatures and any adjusted liquid velocity (see Table 2). Interestingly, the higher CO_2 stripping flux of M5 in comparison with M0 is more pronounced at low tested liquid temperatures (see Table 2). As mentioned previously, the flux of M5 at the liquid temperature of 27 °C and the velocity of 2.8 m s^{-1} was almost 38% higher than the plain membrane. However, the value at the absorbent temperature of 45 °C and 80 °C are 20% and only 9%, respectively. In fact, pore wetting of M5 is lower than M0 at low temperatures because of smaller pore size and higher LEPw, but it seems to become M5 ≥ M0 at high absorbent temperature because of capillary condensation which is promoted by the smaller pore size of M5. The membrane with very small pore size is more susceptible to capillary condensation of water vapor based on the Kelvin equation. Generally, water vapors can condense in channels of sufficiently small dimensions and partially wet the membrane [57]. This mechanism of membrane pore wetting is more crucial when the water vapor forms into the system by increasing temperature and the potential for water vapor re-condensation within the membrane morphology

increases [50]. However, unlike several works on membrane stripping that observed re-condensed water in the gas side, any water droplet was not appeared in the gas side of M5 contactor module in the present stripping experiment. Hence, the fabricated MMMs may show performance stability in long-time stripping operations which will be the focus of our future communications. It can be said that the pore size of membranes utilized at elevated temperature stripping process should be astutely optimized to eliminate both wetting tendency of liquid penetration and absorbent vapor re-condensation into membrane pores.

4. Conclusion

Hollow fiber mixed matrix membranes (MMMs) were successfully fabricated by means of wet phase inversion method when hydrophobic inorganic MMT nano-clay was added to the spinning solutions. The incorporated MMT into PVDF polymer matrix affected phase inversion aspects toward CO_2 stripping performance enhancement. The fabricated membranes were characterized in terms of morphology, gas permeation, surface hydrophobicity and wetting resistance. Physical CO_2 stripping from water by nitrogen as sweep gas was conducted by the gas-liquid membrane contactor and the effect of the liquid velocity and temperature on the performance were investigated. Incorporation of MMT clay particles caused formation of longer finger-like pores together with increase in membrane surface contact angle and wetting resistance. As a result, MMMs exhibited considerably higher stripping performance than the plain PVDF hollow fiber with the best performance obtained when 5 wt% of MMT was added to the polymer. The highest stripping flux for M5 MMM of 4.19×10^{-3} mol m^{-2} s^{-1} at the liquid temperature of 27 °C and liquid velocity of 2.8 m s^{-1} was 38% higher than the plain PVDF. The stripping flux was further enhanced by increasing the temperature of CO_2 rich solution from 27 to 45 and 80 °C, e.g. the

stripping flux of M5 increased from 4.19×10^{-3} to 7.75×10^{-3} mol m^{-2} s^{-1} when the temperature was increased from 27 to 80^{o} at the liquid velocity of 2.8 m s^{-1}.

Nomenclature

A	contact area (m^2)
A_i	inner surface of the hollow fiber membranes (m^2)
C_l	solute gas concentration in liquid (mol m^{-3})
$C_{l,in}$	liquid phase CO_2 concentrations in the inlet of the membrane modules
$C_{l,o}$	liquid phase CO_2 concentrations in the outlet of the membrane modules
C_g	solute gas concentration in gas (mol m^{-3})
ΔC_l^{av}	logarithmic mean of the difference in the concentration of solute gas in liquid phase ($mol\ m^{-3}$)
d_p	pore diameter (m)
d_i	inner diameter of hollow fiber (m)
d_o	outer diameter of hollow fiber (m)
d_{lm}	log mean diameter (m)
H	Henry's constant
J_{CO_2}	CO_2 stripping flux
L	hollow fiber membrane length (m)
L_p	effective pore length (m)
m	molecular weight (g mol^{-1})
p	pressure (pa)
$\overline{p}$	mean pressure (Pa)
$\overline{P}$	total gas permeance (mol m^{-2})

P_p	gas permeance by Poiseuille flow regime (mol m^{-2} Pa^{-1} s^{-1})
P_K	gas permeance by Knudsen flow regime (mol m^{-2} Pa^{-1} s^{-1})
Q_l	liquid flow rate (m^{-1})
r_p	pore radius (m)
$r_{p,m}$	mean pore radius (m)
R	universal gas constant (8.314 J mol^{-1} K^{-1})
T	temperature (K)
V_l	liquid velocity in lumen side (m s^{-1})
ζ	surface porosity
θ	contact angle of liquid and surface
μ	gas viscosity (Pa s)
η	CO_2 stripping efficiency

References

1. A. B. Rao and E. S. Rubin, *Environmental Science & Technology*, 2002, **36**, 4467-4475.
2. P. Kosaraju, A. S. Kovvali, A. Korikov and K. K. Sirkar, *Industrial & Engineering Chemistry Research*, 2004, **44**, 1250-1258.
3. M. Simioni, S. E. Kentish and G. W. Stevens, *Energy Procedia*, 2011, **4**, 659-665.
4. M. Mavroudi, S. P. Kaldis and G. P. Sakellaropoulos, *Journal of Membrane Science*, 2006, **272**, 103-115.
5. R. Wang, H. Y. Zhang, P. H. M. Feron and D. T. Liang, *Separation and Purification Technology*, 2005, **46**, 33-40.
6. A. Mansourizadeh and A. F. Ismail, *Chemical Engineering Journal*, 2010, **165**, 980-988.
7. R. Naim, A. F. Ismail and A. Mansourizadeh, *Journal of Membrane Science*, 2012, **392–393**, 29-37.
8. J.-G. Shim, J.-H. Kim, J. H. Lee and K.-R. Jang, *Energy Procedia*, 2009, **1**, 779-782.
9. M. Rezaei, A. F. Ismail, G. Bakeri, S. A. Hashemifard and T. Matsuura, *Chemical Engineering Journal*, 2015, **260**, 875-885.
10. G. Bakeri, A. F. Ismail, M. R. DashtArzhandi and T. Matsuura, *Journal of Membrane Science*, 2015, **475**, 57-64.
11. S. Koonaphapdeelert, Z. Wu and K. Li, *Chemical Engineering Science*, 2009, **64**, 1-8.
12. F. A. Tobiesen, H. F. Svendsen and K. A. Hoff, *International Journal of Green Energy*, 2005, **2**, 201-215.

13. D. W. Savage, G. Astarita and S. Joshi, *Chemical Engineering Science*, 1980, **35**, 1513-1522.
14. N. Awanis Hashim, Y. Liu and K. Li, *Chemical Engineering Science*, 2011, **66**, 1565-1575.
15. H. Kumazawa, *Chemical Engineering Communications*, 2000, **182**, 163-179.
16. S. Khaisri, D. deMontigny, P. Tontiwachwuthikul and R. Jiraratananon, *Journal of Membrane Science*, 2011, **376**, 110-118.
17. M. Rezaei DashtArzhandi, A. F. Ismail, T. Matsuura, B. C. Ng and M. S. Abdullah, *Chemical Engineering Journal*, 2015, **269**, 51-59.
18. H. Li and H. Kim, *Desalination*, 2008, **234**, 9-15.
19. R. Naim, A. F. Ismail and A. Mansourizadeh, *Journal of Membrane Science*, 2012, **423**, 503-513.
20. M. Rahbari-Sisakht, D. Rana, T. Matsuura, D. Emadzadeh, M. Padaki and A. F. Ismail, *Chemical Engineering Journal*, 2014, **246**, 306-310.
21. S. Husain and W. J. Koros, *Journal of Membrane Science*, 2007, **288**, 195-207.
22. S. A. Hashemifard, A. F. Ismail and T. Matsuura, *Chemical Engineering Journal*, 2011, **170**, 316-325.
23. S. Liu, G. Liu, X. Zhao and W. Jin, *Journal of Membrane Science*, 2013, **446**, 181-188.
24. K. Y. Wang, S. W. Foo and T.-S. Chung, *Industrial & Engineering Chemistry Research*, 2009, **48**, 4474-4483.
25. W. L. Chou, D. G. Yu and M. C. Yang, *Polymers for Advanced Technologies*, 2005, **16**, 600-607.
26. P. Aerts, I. Genne, S. Kuypers, R. Leysen, I. F. J. Vankelecom and P. A. Jacobs, *Journal of Membrane Science*, 2000, **178**, 1-11.
27. P. Aerts, E. Van Hoof, R. Leysen, I. F. J. Vankelecom and P. A. Jacobs, *Journal of Membrane Science*, 2000, **176**, 63-73.
28. O. Monticelli, A. Bottino, I. Scandale, G. Capannelli and S. Russo, *Journal of applied polymer science*, 2007, **103**, 3637-3644.
29. A. Bottino, G. Capannelli, V. D'asti and P. Piaggio, *Separation and Purification Technology*, 2001, **22**, 269-275.
30. A. F. Ismail and A. Mansourizadeh, *Journal of Membrane Science*, 2010, **365**, 319-328.
31. G. Bakeri, A. F. Ismail, D. Rana and T. Matsuura, *Chemical Engineering Journal*, 2012, **198–199**, 327-337.
32. A. Leszczyńska, J. Njuguna, K. Pielichowski and J. R. Banerjee, *Thermochimica Acta*, 2007, **453**, 75-96.
33. A. Olad, *Advances in diverseindustrial applications of nanocomposites, Publisher InTech Europe, Croatia*, 2011, 113-138.
34. P. Wang, J. Ma, Z. Wang, F. Shi and Q. Liu, *Langmuir*, 2012, **28**, 4776-4786.
35. M. Rezaei, A. F. Ismail, S. A. Hashemifard and T. Matsuura, *Chemical Engineering Research and Design*, 2014, **92**, 2449-2460.
36. M. Rezaei, A. F. Ismail, S. A. Hashemifard, G. Bakeri and T. Matsuura, *International Journal of Greenhouse Gas Control*, 2014, **26**, 147-157.
37. K. Yu Wang, T.-S. Chung and M. Gryta, *Chemical Engineering Science*, 2008, **63**, 2587-2594.
38. M. Khayet, C. Y. Feng, K. C. Khulbe and T. Matsuura, *Polymer*, 2002, **43**, 3879-3890.
39. D. Wang, K. Li and W. K. Teo, *Journal of Membrane Science*, 1996, **115**, 85-108.
40. S. Lee, G. Park, G. Amy, S.-K. Hong, S.-H. Moon, D.-H. Lee and J. Cho, *Journal of Membrane Science*, 2002, **201**, 191-201.
41. H. Yasuda and J. T. Tsai, *Journal of Applied Polymer Science*, 1974, **18**, 805-819.
42. M.-J. Han and S.-T. Nam, *Journal of Membrane Science*, 2002, **202**, 55-61.
43. P. Sukitpaneenit and T.-S. Chung, *Journal of Membrane Science*, 2009, **340**, 192-205.
44. H. J. Kim, R. K. Tyagi, A. E. Fouda and K. Ionasson, *Journal of Applied Polymer Science*, 1996, **62**, 621-629.

45. A. Xu, A. Yang, S. Young, D. deMontigny and P. Tontiwachwuthikul, *Journal of Membrane Science*, 2008, **311**, 153-158.
46. A. Razmjou, E. Arifin, G. Dong, J. Mansouri and V. Chen, *Journal of Membrane Science*, 2012, **415–416**, 850-863.
47. Y. Tamai and K. Aratani, *The Journal of Physical Chemistry*, 1972, **76**, 3267-3271.
48. R. N. Wenzel, *Industrial & Engineering Chemistry*, 1936, **28**, 988-994.
49. Garcı, amp, x, M. C. a-Payo, M. A. Izquierdo-Gil and C. Fernández-Pineda, *Journal of Colloid and Interface Science*, 2000, **230**, 420-431.
50. M. Simioni, S. E. Kentish and G. W. Stevens, *Journal of Membrane Science*, 2011, **378**, 18-27.
51. A. Mansourizadeh, *Chemical Engineering Research and Design*, 2012, **90**, 555-562.
52. W. Chinpa, *ScienceAsia*, 2008, **34**, 385-389.
53. G. Bakeri, T. Matsuura, A. F. Ismail and D. Rana, *Separation and Purification Technology*, 2012, **89**, 160-170.
54. A. Mansourizadeh and A. F. Ismail, *Desalination*, 2011, **273**, 386-390.
55. J. Kestin, M. Sokolov and W. A. Wakeham, *Journal of Physical and Chemical Reference Data*, 1978, **7**, 941-948.
56. W. V. Kayser, *Journal of Colloid and Interface Science*, 1976, **56**, 622-627.
57. L. R. Fisher, R. A. Gamble and J. Middlehurst, *Nature*, 1981, **290**, 575-576.